Precision and Radiosonde Validation of Satellite Gridpoint Temperature Anomalies. Part I: MSU Channel 2

ROY W. SPENCER

Earth Science and Applications Division, NASA Marshall Space Flight Center, Alabama

JOHN R. CHRISTY

Atmospheric Science Program, University of Alabama in Huntsville, Huntsville, Alabama

(Manuscript received 9 April 1991, in final form 20 November 1991)

ABSTRACT

In Part I of this study, monthly 2.5° gridpoint anomalies in the *TIROS-N* satellite series Microwave Sounding Unit (MSU) channel 2 brightness temperatures during 1979–88 are evaluated with multiple satellites and radiosonde data for their climate temperature monitoring capability. The MSU anomalies are computed about a 10-year mean annual cycle at each grid point, with the MSUs intercalibrated to a common arbitrary level. The intercalibrations remove relative biases between instruments of up to several tenths of a degree celsius. The monthly gridpoint anomaly agreement between concurrently operating satellites reveals single-satellite precision generally better than 0.07°C in the tropics and better than 0.15°C at higher latitudes. Monthly anomalies in radiosonde channel 2 brightness temperatures computed with the radiative transfer equation compare very closely to the MSU measured anomalies in all climate zones, with correlations generally from 0.94 to 0.98 and standard errors of 0.15°C in the tropics to 0.30°C at high latitudes. Simplification of these radiative transfer calculations to a static weighting profile applied to the radiosonde temperature profile leads to an average degradation of only 0.02° in the monthly skill. In terms of a more traditionally measured quantity, the MSU channel 2 anomalies match best with either the radiosonde 100–20-kPa or 100–15-kPa layer anomalies. No significant spurious trends were found in the 10-yr satellite dataset compared to the radiosondes that would indicate a calibration drift in either system. Thus, sequentially launched, overlapping passive microwave radiometers provide a useful system for monitoring intraseasonal to interannual climate anomalies and offer hope for monitoring of interdecadal trends from space. The Appendix includes previously unpublished details of the MSU gridpoint anomaly dataset construction. Part II of this study addresses the removal from channel 2 of the temperature influence above the 30-kPa level, providing a sharper and thus potentially more useful weighting function for monitoring lower tropospheric temperatures.

1. Background

The potential of externally calibrated microwave radiometers for precision monitoring of climate change was demonstrated by Spencer and Christy (1990, hereafter SC) and Spencer et al. (1990, hereafter SCG) in the context of deep-tropospheric and lower-stratospheric brightness temperature (T_b) anomalies. With an instrument calibration totally independent of any radiosonde data, intercomparisons between simultaneously operating Microwave Sounding Units (MSUs) on morning and afternoon *TIROS-N* satellites revealed agreement to 0.01°C for monthly, globally averaged T_b anomalies and instrument stability to better than 0.01°C over a 2-year overlap period. While a precision of 0.01°C might seem implausible in view of the MSU single-sample instrumental noise of 0.3°C, a month's worth of global observations involves many (10^6) measurements. This would reduce the noise to 0.0003°C if the measurement errors are randomly distributed, but the different space and time sampling characteristics of the concurrently operating morning and afternoon satellites degrade the precision to 0.01°C. Whereas the previously published results addressed the precision of the satellite measurements on hemispheric and global scales, we now extend this evaluation to the 2.5° gridpoint scale where individual radiosonde stations can be used as an independent tool for verifying the satellite data quality.

A fundamental question often asked is, What do the channel 2 T_b anomalies represent? First let us address the deep-layer nature of the measurement. The channel 2 weighting function (Fig. 1) is vertically broad and represents the vertical distribution (in $\log_e p$ coordinates) of the satellite-measured radiation over a layer extending from the surface to above 30 kPa. The bulk of this microwave radiation is thermally emitted by molecular oxygen with an intensity, via the Planck

Corresponding author address: Dr. Roy Spencer, ES43 Earth Science and Applications Division, NASA Marshall Space Flight Center, Alabama 35812.

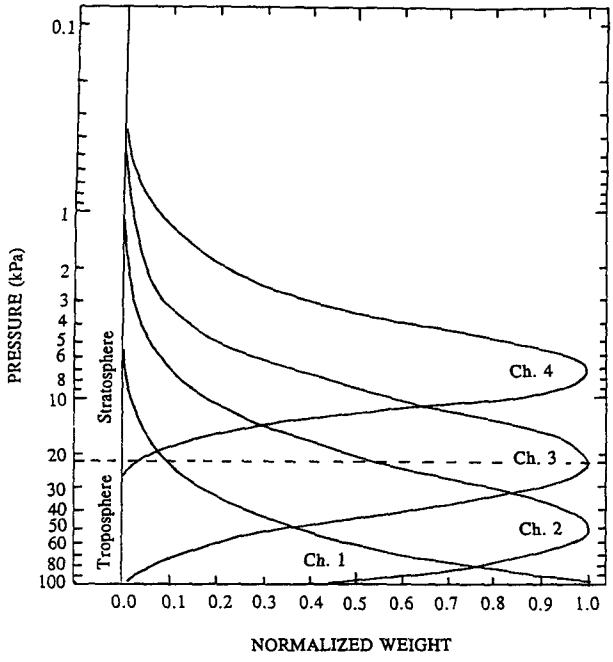

FIG. 1. Weighting functions for MSU channels 1 (50.3 GHz); 2 (53.74 GHz); 3 (54.96 GHz); and 4 (57.95 GHz) for a 22° view angle through the *U.S. Standard Atmosphere.*

equation, directly proportional to temperature. Oxygen is an ideal temperature tracer for climate monitoring because it occupies a large fraction of our atmosphere (20.95% by volume), is uniformly mixed, and its concentration is very stable in time. Therefore, MSU channel 2 measurements are dominated by the vertically weighted air temperature through a deep tropospheric layer of air. In typical satellite sounder "retrieval" schemes, this deep-layer measurement is combined with other channels having overlapping weighting functions (such as MSU channels 1, 3, and 4 in Fig. 1) in order to deconvolve these weighting functions into an "averaging kernel" (see Conrath 1972; Grody 1980), which is considerably sharper than the individual channel-weighting functions. However, one rapidly approaches a practical limit in the ability to sharpen the averaging kernel because of the finite number of channels, each having a certain amount of measurement noise that is amplified in the retrieval process. Therefore, based upon current theoretical and engineering limits, the satellites simply cannot measure the many levels a radiosonde system measures. Thus, even though satellite temperature retrievals often relate the measurements to temperature at a specific level in the atmosphere, such a retrieval is ultimately based upon statistically averaged or recently observed radiosonde-measured relationships that occur in the atmosphere and does not change the fact that the satellite can only measure deep-layer averages.

A second issue concerns how much of the satellite-derived anomaly is contaminated by nonoxygen emission. Based upon theory (see SCG), the MSU channel 2 T_b anomalies are expected to have small contaminating influences from interannual variations in precipitation-size ice in deep convection, cloud water, water vapor, and surface emissivity. However, the magnitudes of these errors are difficult to quantify without knowledge of interannual variations in these variables. Theoretical evidence was presented by SCG to support interpretation of the T_b anomalies as dominated by thermometric temperature to about 0.01°C for globally averaged monthly anomalies, although regional areas might experience contaminating influences exceeding 0.1°C. For instance, for water vapor thermal emission, SCG computed that 20% deviations from the average water vapor abundance can cause up to 0.03°C contamination of tropical oceanic channel 2 measurements. Probably the largest contaminating influence is from precipitation-size ice in deep convective systems (e.g., Grody 1983). This type of contamination, although affecting a small percentage of the observations, can cause T_b depressions of up to several degrees. After applying a screening procedure for deep convection (described below), it is the interannual variations in the deep convective signatures remaining in our data that will cause contamination of the anomalies.

Therefore, at this point we hypothesize that the channel 2 anomalies are dominated by thermometric temperature variations over a layer represented by the channel 2 weighting function. However, theory alone is insufficient for rigorous evaluation of the satellite temperature monitoring technique. Here we will present results of comparisons between 10 years of monthly radiosonde thickness anomalies to the MSU channel 2 anomalies in atmospheric environments ranging from tropical to polar. If it can be demonstrated that individual gridpoint anomalies in MSU channel 2 T_b closely match anomalies in radiosonde measurements, then we will have increased confidence that the full global 2.5° gridpoint dataset can be successfully utilized for intraseasonal to interannual climate studies in regions not well sampled by radiosondes. Furthermore, if there is little or no 10-year trend in the difference between the radiosonde and satellite time series, then the satellite system will be supported for long-term monitoring (e.g., of potential global warming).

2. Limits of radiosonde precision for gridpoint climate monitoring

Before gridpoint comparisons with radiosonde data are carried out, it is useful to address the capability of a single radiosonde station to measure monthly anomalies in different layers, as well as to measure decadal trends.

a. Monthly radiosonde precision

Individual radiosonde temperature profiles are generally considered to have about a 0.4°C random error

in the calibration of the sonde. If a station makes 60 observations per month, then that station's precision in the measurement of a monthly temperature anomaly is $(0.4/(60)^{1/2})$, or about 0.05°C, which is negligibly small. However, the fact that each measured profile might not accurately represent the larger-scale environment will produce an additional source of error for climate monitoring that related to temperature variability on the micro- and mesoscale. (While other errors induced by solar heating and infrared cooling of the temperature sensor are also expected, these should average out over the course of a month, keeping in mind that we are not as interested in absolute accuracy as we are in anomalies from a mean value.) The spatial variability error is a difficult error to quantify since we do not know how temperatures vary on all space scales within a mesoscale region over the course of a month. It seems reasonable that thunderstorm-induced air temperature changes would approach 1.0°C on occasion, which would not be representative of the larger-scale environment. It is unclear, however, how such effects would average out over one month.

Because of the difficulty in a priori estimation of the radiosonde errors in monthly anomaly measurements, we have chosen two pairs of closely spaced tropical western Pacific Ocean stations to see what level of agreement is experienced between them. These are 1) Yap and Koror islands and 2) Truk and Ponape islands. The tropical environments were chosen to minimize horizontal gradients in the monthly anomalies. The distances between these station pairs are 450 km and 700 km, respectively. In Fig. 2 the agreement between these station pairs is plotted in terms of correlations and standard errors of estimate for different layers' thicknesses. Note that the agreement between stations is about 0.2°C. This would be a conservative estimate of a single station's precision, since it would also include some real difference in the anomalies between the two stations. As a move is made toward midlatitude regions where there exists greater variability in air masses, we can expect the 0.2° precision of a single station to degrade. This is due to greater variability of the atmosphere in space and time, which would be that much harder for the station to capture.

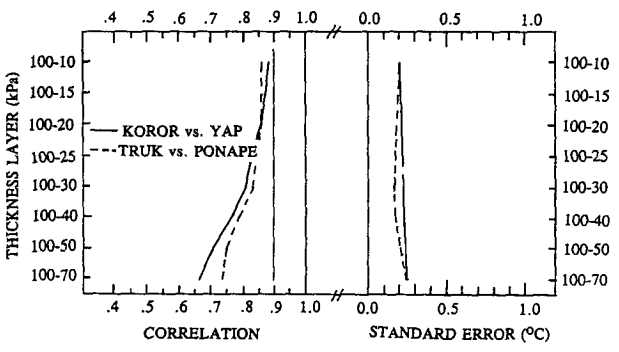

FIG. 2. Monthly temperature anomaly agreement between closely spaced tropical Pacific radiosonde stations for different thickness layers.

b. Ten-year trends

When the 10-year trends of the layer temperatures are plotted for these station pairs (Fig. 3), we see disturbingly large differences of 0.2°–0.5°C for the period 1979–88. If two other western Pacific stations, Guam and Majuro, are also examined, we find somewhat less disagreement. Whatever the reasons for such large variability in single-station trends, it appears that decadal trends calculated from a single radiosonde station should be used with extreme caution. If this station-to-station variability is random in nature, then many-station averages might be more confidently related to real atmospheric temperature trends (as we will see below). From Fig. 3, about a 0.1°–0.2°C limit to the agreement in decadal trends might be expected between the satellite and several stations averaged together, and up to 0.5°C disagreement for individual station comparisons.

3. Satellite gridpoint dataset construction and precision

a. Limb correction and gridpoint assignment

The MSU measures at 11 scan angles as it scans across the satellite subtrack every 9.5° from 47° left to 47° right of nadir (see SCG for more information regarding the MSU sampling geometry). Each scan position (footprint) was calibrated as a T_b according to the procedure in SCG. This involves linear interpolation between the radiometer measurement of the cosmic background (assumed to be 2.7 K) and a warm target whose temperature is monitored with redundant platinum resistance thermometers. After calibration, regression-derived limb correction equations were applied to all ten nonnadir scan positions data to correct for the off-nadir T_b being colder than the nadir T_b. This relative coldness (often called "limb darkening") is due to the off-nadir weighting functions being slightly higher in the troposphere than the nadir-weighting function. These limb correction equations have the form

$$T_{bL} = aT_b - b, \tag{1}$$

where T_{bL} is the limb corrected T_b for an individual MSU scan position, and the regression coefficients constants a and b were derived as a function of satellite, 10° latitude band, and scan position. Approximately 6700 scans were chosen from each of 12 calendar months for each satellite for certain years, that is *TIROS-N* (1979); *NOAA-6* and *NOAA-7* (1982); *NOAA-9* (1986); and *NOAA-10* and *NOAA-11* (1990). Each scan was carefully chosen to have little evidence of horizontal (synoptic scale) temperature gradients,

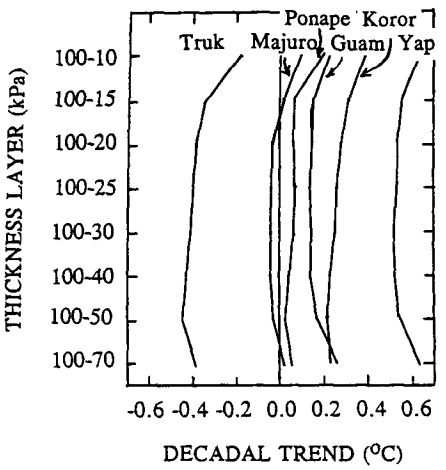

FIG. 3. Same as in Fig. 2 but for decadal trends for each station.

with the difference in the T_b from opposite ends of the scan line not exceeding a few degrees. This maximizes the limb-darkening effect compared to the horizontal temperature gradient effect. For each satellite, all 12 months of data (80 000 scan lines) were partitioned according to which 10° latitude band each occupied (assigned by the nadir scan position). Both northern and southern latitude bands were combined together to avoid averaging biases arising from a single scan position usually being on the warmer (tropical) or colder (polar) side of the nadir footprint. The resulting limb-corrected T_{bL} for the first (number 1) and last (number 11) scan positions were quite noisy, so they were excluded in any further processing of the data.

Next, T_{bL} in scan positions 3–9 were checked for deep-convective ice signatures, which appear as localized T_{bL} depressions of up to several degrees. Between 50°N and 40°S latitudes, we excluded any T_{bL} that was more than 0.5°C cooler than a linearly interpolated T_{bL} computed for that location from the warmest T_{bL} found on both sides of the print in question.

Next, each T_{bL} was binned into the appropriate 2.5° grid square according to the latitudes and longitudes provided with the raw data by NESDIS. This was done on a daily basis for each satellite separately and for ascending and descending satellite passes separately. At the end of each day, a simple (one per distance) interpolation was performed to empty 2.5° grid squares for ascending and descending grid fields separately with the nearest nonzero grid data, in the east and west directions out to a maximum distance of 15 grids. These interpolated ascending and descending T_{bL} fields were then averaged together to provide a single daily T_{bL} field for each satellite. At the end of each month, a time interpolation was performed (±2 days) to any remaining empty grid squares. The daily fields were then averaged together to produce monthly grid fields. Further references to the averaged fields will always assume the limb-correction procedure was applied to the calibrated data (T_{bL}), so for brevity the data will now be referred to as simply T_b.

b. Gridpoint-anomaly calculation

Production of monthly gridpoint T_b anomalies would be a simple procedure if a single satellite had been operating for the full period of the satellite record. This would have involved computing, say, a 10-year average for each of the 12 calendar months at every gridpoint and then subtracting this average from individual months within the 10-year period. Unfortunately, there are two complications that must be taken into account.

First, the satellite record is made up of seven satellites (six of which we use, see Fig. A1), all of which have calibration biases relative to each other by up to several tenths of a degree. The second complication is the existence of two separate orbit times alternating throughout the satellite record. Because MSU channel 2 has some sensitivity to diurnal variations in land surface heating, the gridpoint averages are dependent upon the satellite orbit time (0230 or 0730) and the local strength of the diurnal heating cycle, which is a function of geography and time of year.

The procedure for the merging of all six satellites' data records into a single time series of anomalies is described in the Appendix. This is the same procedure that led to the global time series reported by SC and SCG, but some details of which have been previously undocumented.

c. Gridpoint precision and signal to noise

Monthly gridpoint precision can be evaluated by computing and comparing anomalies from separate satellites for months when two satellites are simultaneously operating. A map of the calculated single-satellite standard deviation from a 20-month overlap between *NOAA-6* and *NOAA-7* (Fig. 4a) shows excellent agreement. Note that most areas have gridpoint T_b agreement to better than 0.07°C, mainly in the tropics, with almost all other nontropical areas exhibiting better than 0.15°C agreement. Degradation of a few hundredths of a degree is seen over land areas. This noise is probably introduced by the different diurnal variations in the surface as seen by the morning (*NOAA-6*) and afternoon (*NOAA-7*) satellites. A few small areas of mountainous terrain (Andes, Himilayas, Tibetan Plateau, and portions of Greenland and Antarctica) show poorer agreement between satellites due to enhancement of this surface influence as the terrain protrudes up into the channel 2 weighting function.

How these errors compare to typical signal strength in different regions is revealed in Fig. 4b, where the

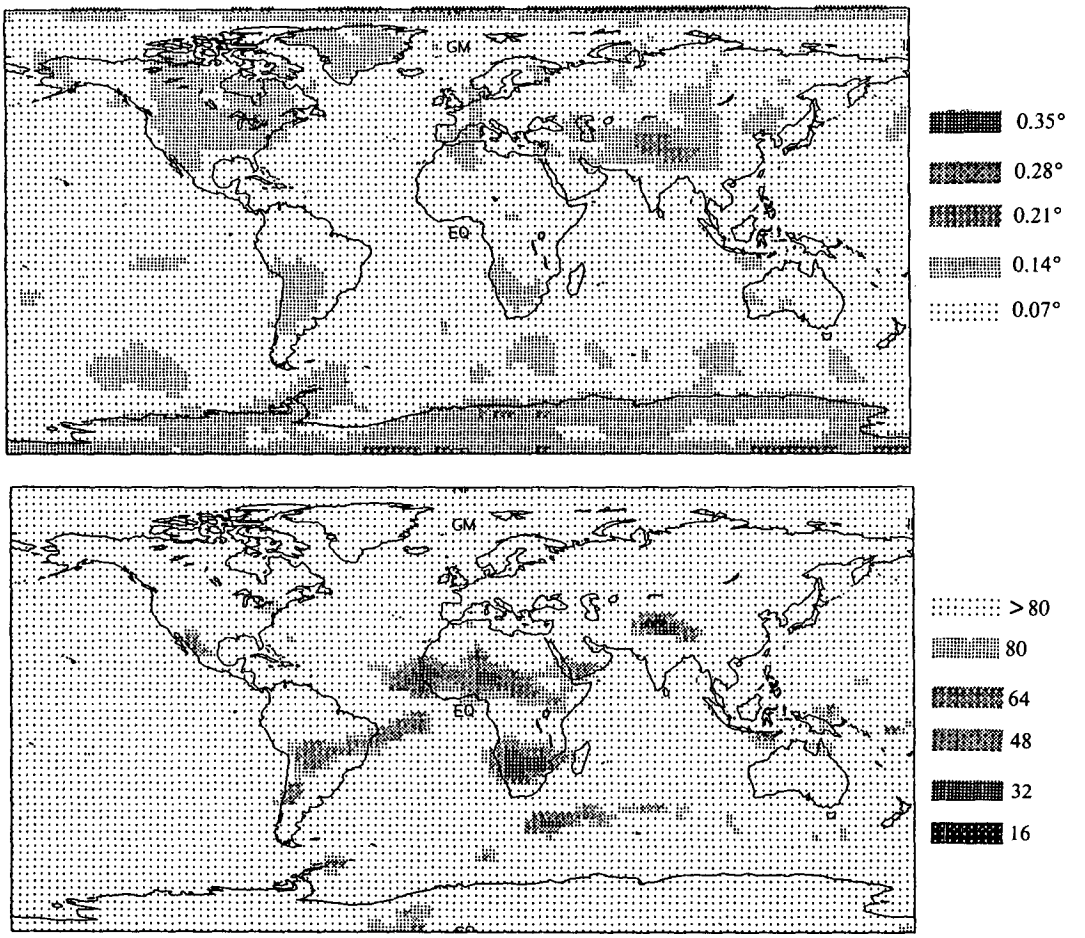

FIG. 4. The standard deviation (top) and signal/noise (bottom) of the MSU channel 2 gridpoint anomaly differences (°C) between *NOAA-6* and *NOAA-7* for a 20-month overlap period, resulting from the satellite intercalibration procedure outlined in the Appendix.

signal-to-noise ratios {S/N = [variance (intersatellite anomaly sums)]/[variance (intersatellite anomaly differences)]} are displayed. It is seen that the channel 2 S/N is over 80 for most of the earth and drops below 50 for a few small regions. This suggests that MSU channel 2 can monitor T_b variations to a high level of precision, even at the 2.5° gridpoint level.

4. Radiosonde comparisons

While the preceding results demonstrate precision in the ability of a single MSU to precisely monitor monthly gridpoint anomalies in channel 2 T_b, it still remains to be demonstrated that these anomalies are dominated by a temperature signal. We will address three kinds of radiosonde comparisons to MSU measured anomalies: 1) channel 2 T_b computed from the radiosonde profiles of temperature and humidity with the radiative transfer equation (see Grody 1983), 2) a much simpler method where an assumed constant weighting function is applied to the radiosonde temperature profile only, and 3) comparisons to traditionally measured thickness anomalies for various standard atmospheric layers.

a. Radiosonde data processing

The channel 2 T_b anomalies from the merged multisatellite dataset at specific 2.5° grid squares (described in the Appendix) were compared to radiosonde measurements for individual stations within those grid squares. The radiosonde data utilized for our intercomparisons is a quality-controlled dataset provided by NCAR. The stations are United States controlled and include, in addition to the mainland United States, scattered Pacific, Caribbean basin, and Alaska locations. Of approximately 120 stations that have fairly complete 10-year records, here we will present the results from six stations representing various climate regimes (Table 1). Also, comparisons to several stations

TABLE 1. Radiosonde stations from various climatic regimes chosen for comparison to the satellite gridpoint temperature anomaly dataset.

Station	Climatic type	Location
Cold Bay, Alaska	Polar	55.2°N, 162.7°W
St. Cloud, Minnesota	Continental	45.6°N, 94.2°W
Oakland, California	Midlatitude	37.7°N, 122,2°W
Lihue, Hawaii	Subtropical	22.0°N, 159.3°W
San Juan, Puerto Rico	Subtropical	18.4°N, 66.0°W
Guam	Tropical	13.6°N, 144.8°E

from each of these six regimes are composited together to provide regionally averaged comparisons.

In the first type of radiosonde comparison, the radiative transfer equation (Grody 1983) was used to compute a T_b from the temperature and water vapor information measured by the radiosonde. All radiosonde ascents were included that went above 10 kPa, with the most recent radiosonde data above 2 kPa (usually not more than 1 or 2 days old) being inserted if the current profile did not go above 2 kPa. Each sounding was capped by an artificial temperature of 250 K at 0.01 kPa. These T_b computations throughout the 10-year period were averaged on a monthly basis. The 10-year (1979–88) monthly averages were then subtracted from the individual monthly averages to arrive at a 10-year time series of monthly anomalies for each station.

Second, a simpler method of computing T_b was used that avoids the computational intensity of the radiative transfer equation. Because the temperature dependence of the oxygen absorption and the water vapor absorption are both small, a static weighting function can be applied to just the temperature profile without risking great error. The channel 2 weighting function for the *U.S. Standard Atmosphere* (Fig. 1) was applied to the radiosonde temperature profiles to provide a vertically weighted T_b estimate, that is,

$$\hat{T}_b = \frac{\sum_{i=1}^{N} w_i T_i \log_e(p_1/p_2)}{\sum_{i=1}^{N} w_i \log_e(p_1/p_2)}, \qquad (2)$$

where the ith layer of N radiosonde profile layers has an average temperature (T_i), an average weight (w_i) from Fig. 1, and bounding pressures (p_1 and p_2).

Third and last, comparisons were made to all combinations of thickness layers having bases at 100 kPa or 85 kPa and tops at 70, 50, 40, 30, 25, 20, 15, and 10 kPa. Because virtually all of the correlations were somewhat lower for layers having bases at 85 kPa, only the results for the layers having 100-kPa bases are presented here.

b. *Single-station gridpoint correlations*

The levels of agreement between the satellite measurements at each of the six stations are presented in Figs. 5–10 in terms of correlation coefficients (R) and standard error of estimate (SE) of the radiosonde temperature anomalies. The first half of these figures (a) shows the time series of comparisons to radiosonde-computed channel 2 T_b anomalies, while the second half (b) shows R and SE for various thickness-layer temperature anomalies.

In Cold Bay, Alaska (Fig. 5a), we find a monthly correlation of 0.97 between the satellite-measured and the radiosonde-calculated T_b anomalies, with a corresponding standard error (SE) of 0.24°C. The yearly anomaly correlation is just under 0.99. Use of the simplified T_b computations with Eq. (2) results in $R = 0.96$ and SE = 0.28°C, only a slight degradation in performance for the monthly anomalies. The best monthly agreement between the satellite and a traditionally measured thickness layer (Fig. 5b) is with the 100–20-kPa layer ($R = 0.94$), which is not quite as good as with the other measures. Most of the stations examined (over 100 in number) indicated the 100–20-kPa or

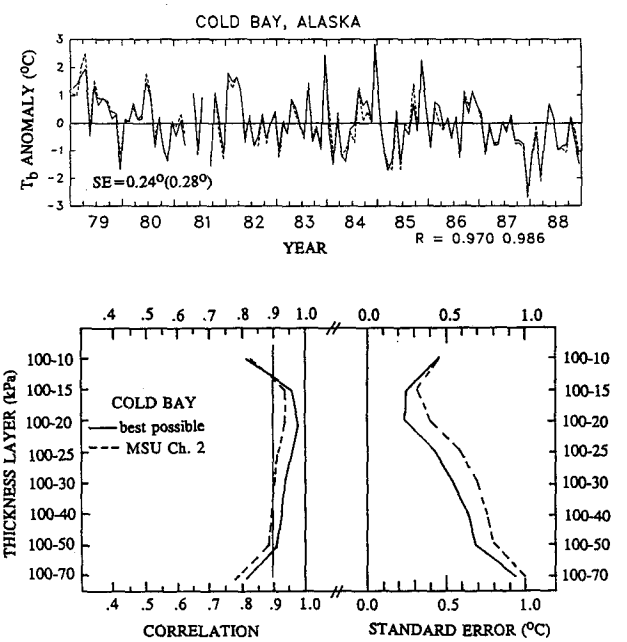

FIG. 5. Time series (a) of MSU channel 2 anomalies and radiosonde-calculated channel 2 anomalies; and correlation and standard errors (b) with radiosonde thickness temperature anomalies for Cold Bay, Alaska, during 1979 through 1988. In (a) the solid line is MSU-measured, the dashed line is radiosonde-measured, and the correlations (R) are for the monthly and yearly anomalies, respectively. In (b) the solid line shows the best agreement possible based upon MSU channel 2 T_b being computed from the radiosonde data, and the dashed line shows the satellite-measured agreement with the radiosonde thickness temperature anomalies.

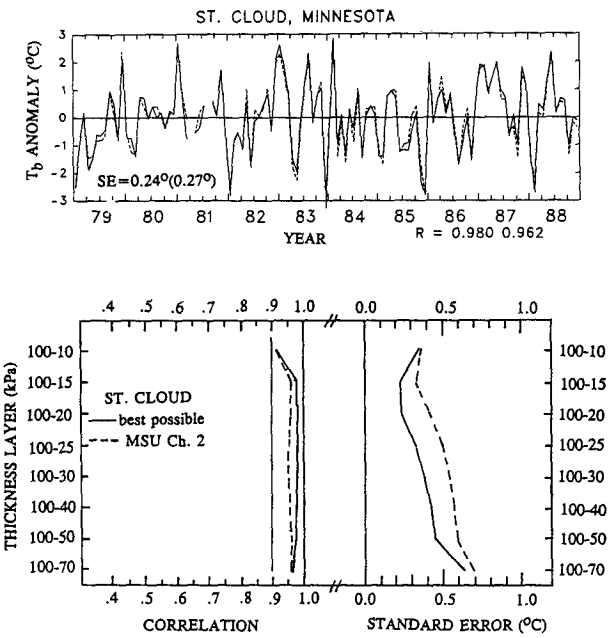

FIG. 6. As in Fig. 5 but for St. Cloud, Minnesota.

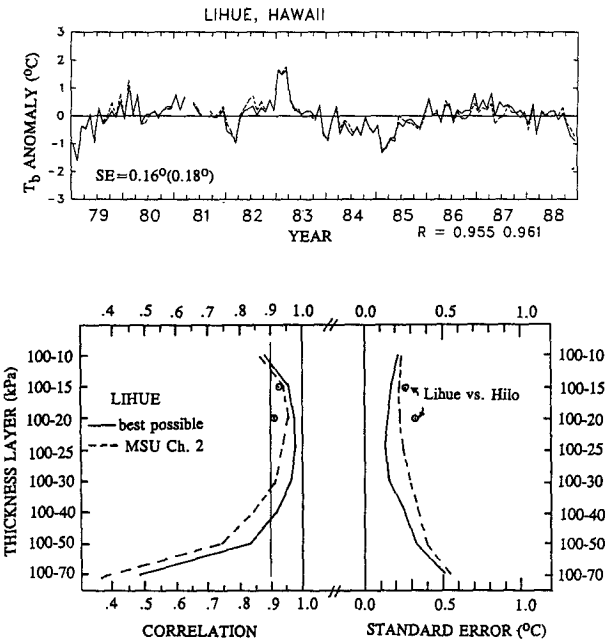

FIG. 8. As in Fig. 5 but for Lihue, Hawaii. Also shown in (b) is the level of agreement between Hilo, Hawaii, and Lihue, Hawaii.

100–15-kPa layer as having the best agreement of all traditionally measured thickness layers. This should not be surprising considering the channel 2 weighting function distribution in Fig. 1.

In St. Cloud, Minnesota (Fig. 6a), we find similar results to those of Cold Bay, with a monthly correlation of 0.98 and SE of 0.24°C. Use of Eq. (2) gives only slightly degraded results with $R = 0.97$ and SE = 0.27°C. These figures are slightly better than the correlation with the 100–15-kPa layer ($R = 0.96$) in Fig. 6b.

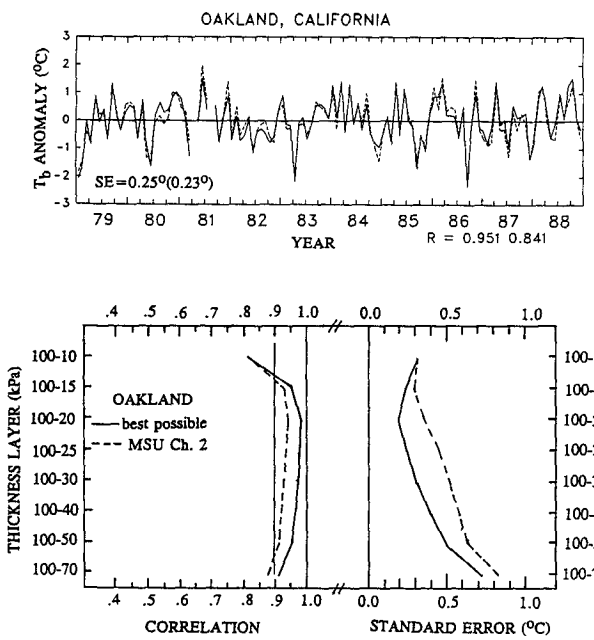

FIG. 7. As in Fig. 5 but for Oakland, California.

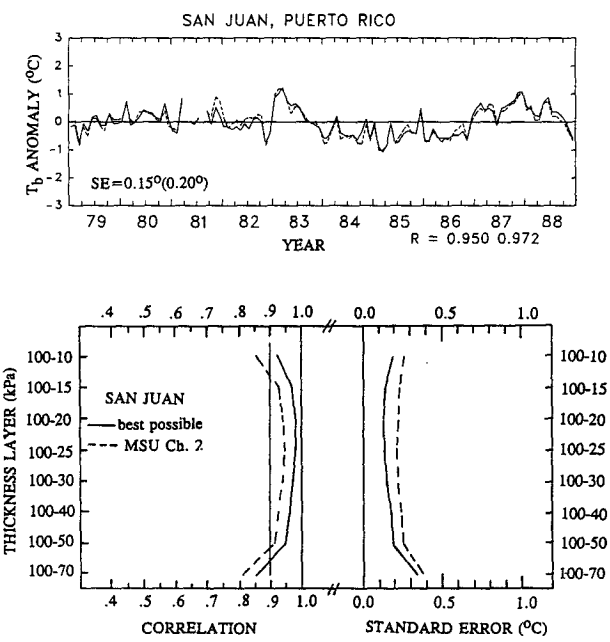

FIG. 9. As in Fig. 5 but for San Juan, Puerto Rico.

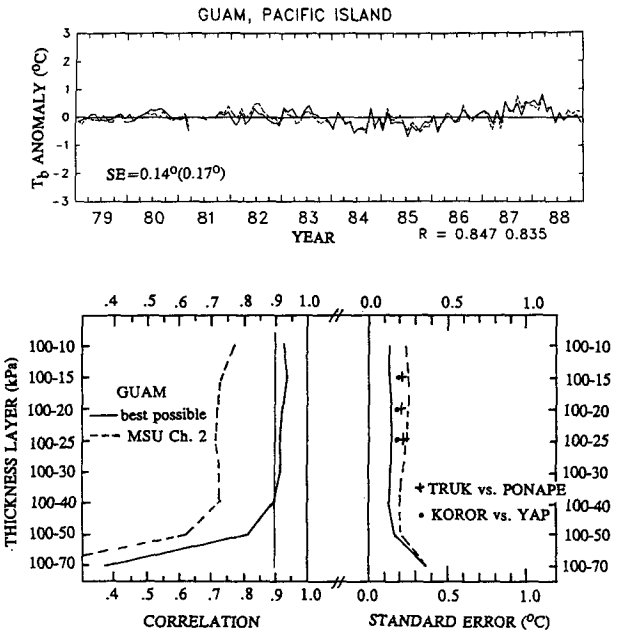

FIG. 10. As in Fig. 5 but for Guam.

The comparisons to radiosonde-computed channel 2 for Oakland, California (Fig. 7a), reveal $R = 0.95$ and SE = 0.25°C. Interestingly, the results with Eq. (2) are slightly better than those obtained with the radiative transfer equation, with SE = 0.23°C. As with the other stations, these are both slightly better than with the thickness layer of best agreement (100–20 kPa) for which $R = 0.94$ (Fig. 7b).

At Lihue, Hawaii (Fig. 8a), the radiative transfer calculations with the radiosonde data show a 0.96 correlation and SE = 0.16°. With Eq. (2) these measures become $R = 0.95$ and SE = 0.18°C, again revealing the utility of a simple vertically weighted average of the temperature profile with a constant weighting function. Compared to a traditionally measured layer, best agreement is seen in the 100–20-kPa layer, with $R = 0.95$ and SE = 0.23°C (Fig. 8b). Note that we are now reaching the limit of agreement (0.20°C) between adjacent tropical radiosonde stations measuring the same layers shown in Fig. 2. In fact, comparison between the Lihue and Hilo, Hawaii, radiosonde stations, despite their proximity to each other, yields *poorer* agreement (the circles in Fig. 8b) than the satellite shows with Lihue. This casts some doubt on the regional representativeness of isolated radiosonde stations when used to construct "global" temperature anomalies. Of some interest are the low correlations between the MSU channel 2 anomalies and the lower tropospheric temperature anomalies at Lihue. This illustrates very little coupling between the lower and middle troposphere in this oceanic region.

The agreement with the satellite anomalies at San Juan, Puerto Rico (Fig. 9a), is about the same as was found in Hawaii, with $R = 0.95$ and SE = 0.15°C. Using Eq. (2) for the radiosonde computations, we once again obtain only slightly poorer performance, with $R = 0.93$ and SE = 0.20°C. In the comparisons to thickness anomalies (Fig. 9b) for the 100–25-kPa layer, $R = 0.95$ and SE = 0.21°C. Again, these levels of agreement approach the precision inherent in the sampling provided by a single radiosonde station.

Guam, in the tropical western Pacific (Fig. 10a), reveals a somewhat lower correlation ($R = 0.85$) but an excellent standard error (SE = 0.14°C). The low correlation reflects the very weak signal of monthly temperature anomalies in this region of the world. Note that the correlation is no worse than that between the adjacent radiosonde stations in Fig. 2. The constant weighting method [Eq. (2)] gives $R = 0.81$ and SE = 0.17°C, again only a slight degradation from using the full radiative transfer equation. Considerably worse results are revealed for the 100–15-kPa layer anomalies, where $R = 0.74$ and SE = 0.25°C. This degradation is the result of low natural interlayer correlations within the tropical troposphere at Guam, which makes comparison with the correct vertical weighting profiles very important.

c. *Composite station correlations*

The levels of agreement improve further when the satellite–radiosonde comparisons are grouped by region, with several station anomalies (and the corresponding satellite anomalies at those locations) averaged together each month (Table 2). The largest improvement in correlation is seen for the tropical western Pacific, for which Guam was 0.85; and now a six-station composite correlation increases to 0.95, with the SE

TABLE 2. Station composite correlations and standard errors of satellite versus radiosonde monthly anomalies in channel 2. Numbers in parentheses are the corresponding single-station values from the stations represented in Figs. 5–10.

Region	R	SE
Alaska (15)	0.98 (0.97)	0.17° (0.24°)
Great Lakes (6)	0.98 (0.98)	0.22° (0.24°)
West Coast (4)	0.97 (0.95)	0.18° (0.25°)
Caribbean (6)	0.97 (0.95)	0.10° (0.15°)
West Pacific (7)	0.95 (0.85)	0.09° (0.14°)

Alaska: (15) Anette, Yakutat, Kodiak, King Salmon, Cold Bay, Adak, St. Paul Island, Anchorage, Fairbanks, McGrath, Bethel, Kotzebue, Nome, Barter Island, Barrow. Great Lakes: (6) Sault Ste. Marie, MI; International Falls, MN: Green Bay, WI; St. Cloud, MN; Huron, SD. West Coast: (4) Quillayute, WA; Salem, OR; Oakland, CA; San Diego, CA. Tropical West Pacific: (7) Koror, Yap, Majuro, Wake, Guam, Truk, Ponape. Caribbean: (6) Christ Church, Barbados; Santo Domingo, Dominican Republic; Piarco, Trinidad; San Juan, Puerto Rico; Curacao, Netherland Antilles; Roberts, Cayman Islands.

improving to 0.09°C. These station composites thus reveal that the radiosonde (and satellite) noise at individual grid points is reduced when several grid points are averaged together. This suggests that regional MSU-measured anomalies are somewhat more accurate than individual gridpoint anomalies.

d. *Trends*

Table 3 shows the 10-year trends for these station composites as well as the satellite-measured trends. A net disagreement of 0.05°C is found for all 38 stations combined. If the stations' trend errors were independent, this would correspond to an average single-station trend error of 0.3°C, consistent with the disagreement between adjacent stations shown in Fig. 3 (which we recall is an underestimate of the high-latitude trend errors, where much larger interannual variability exists). This does not mean that the MSU decadal trends at individual grid points are accurate, only that the radiosonde data are probably not sufficiently good enough to determine the level of trend error in the MSU gridpoint (and thus regional or global) trends.

5. Conclusions

Radiosonde comparisons support the use of satellite passive microwave T_b measurements for deep-layer temperature monitoring at the 2.5° gridpoint scale. Intersatellite comparisons of monthly *TIROS-N* MSU channel 2 T_b anomalies at the 2.5° gridpoint level reveal remarkable agreement, generally better than 0.07°C in the tropics and 0.15° at high latitudes. Comparisons between MSU-observed and radiosonde-calculated monthly anomalies in channel 2 T_b reveal correlations generally around .95 and standard errors from 0.15°C in the tropics to 0.25°C at high latitudes. The standard errors degrade by an average of only 0.02°C if a simple vertical weighting is applied to the radiosonde temperature profiles, instead of using radiative transfer calculations on the full temperature and humidity profiles. This simple method is recommended for quantitative comparisons to other multiple-layer temperature datasets (e.g., model output). Compositing of 4 to 15 radiosonde stations together in specific regions improves the satellite–radiosonde agreement to 0.10°C in the tropics and to about 0.20°C at high latitudes. Thus, the satellite precision approaches that of individual radiosonde stations in their ability to measure monthly temperature anomalies, which we estimate to be 0.2°C from intercomparisons of closely spaced tropical oceanic stations in the Pacific. In terms of traditionally measured layers, the highest satellite correlations exist for the 100–20-kPa layer or the 100–15-kPa layer. These correlations are only slightly poorer than for the channel 2 weighting profile, except over the tropical Pacific where natural interlayer correlations are low, making the correct weighting of the radiosonde profile very important.

We find no evidence of instrumental drift in the 10 years of MSU channel 2 measurements (1979–88) at the level of our ability to measure it with multiple-station radiosonde data.

TABLE 3. Decadal trends (°C, for 1979–88) in MSU-observed and radiosonde-computed channel 2 T_b anomalies for the regional station composites listed in Table 2. The number of stations in each group is shown in parentheses.

Region	Radiosonde Channel 2 trend	MSU Channel 2 trend	(Raob-MSU)
Alaska (15)	−0.67°	−0.67°	0.00°
Great Lakes (6)	+0.33°	+0.39°	−0.06°
West Coast (4)	−0.03°	+0.20°	−0.23°
Caribbean (6)	−0.01°	+0.12°	−0.13°
West Pacific (7)	+0.14°	+0.09°	+0.05°
Weighted average (38)			−0.05°

Acknowledgments. We thank Roy Jenne and Dennis Joseph at NCAR for provision of the raw MSU datasets and radiosonde data. Robbie Hood assisted in the processing of the radiosonde data and radiative transfer modeling. Norm Grody (NOAA/NESDIS) and Shelby Tilford (NASA Headquarters) provided useful advice during the course of this study.

APPENDIX

Merging of Multisatellite MSU Data for Regional Climate Monitoring

The *TIROS-N* series of sun-synchronous polar-orbiting satellites has provided continuous temperature monitoring of the atmosphere since late 1978. Each satellite has an operational lifetime of one to three years, although *NOAA-6* operations spanned seven years. Nominally two satellites are operated at the same time, one in a morning orbit (0730) and one in an afternoon orbit (1430), although a few periods have existed when only a single satellite has been available. Launches of new satellites alternate between morning and afternoon orbits.

If a single satellite had always been operated (and its sensors remained sufficiently stable), then computation of monthly gridpoint brightness temperature anomalies from this single satellite would have been a simple process of averaging all data into monthly 2.5° bins for some multiyear period sufficient to observe a representative annual cycle (say 1979–88) and then subtracting this average from the individual single-month averages to arrive at a time series of monthly

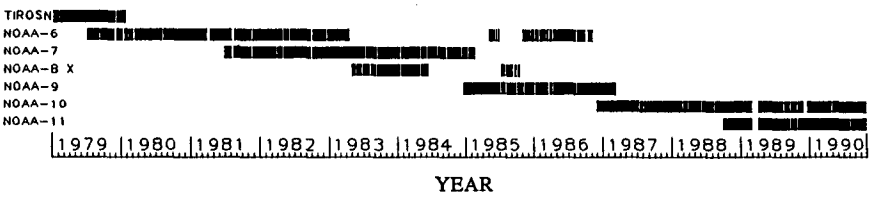

FIG. A1. Periods of operation and overlap between MSUs during 1979–90. Gaps indicate one or more days of less than 85% global data. March 1989 data was not yet available for this dataset.

anomalies. Unfortunately, we must deal with multiple satellites with slightly different sensors in different orbits. As a consequence, merging of the data from these overlapping satellites into a continuous time series requires the removal of two basic sources of differences between satellites. First is the absolute calibration differences between different MSUs, which can be several tenths of a degree celsius. The second arises from the different solar times of the morning and afternoon orbits. MSU channel 2 has some sensitivity to the surface, and so the 1430 channel 2 T_b observations over land can be considerably warmer than either the 0730 or 1930 T_b. This effect is regionally dependent and becomes stronger as one moves toward the equator and higher elevations. For example, we see 5°–10°C diurnal range over portions of the United States and 10°–15°C over the Sahara desert. Therefore, removal of an annual cycle for anomaly computation must be done separately for different orbit times and different locations.

Although different paths can be followed, resulting in only minor changes in the final results, these are the specific steps performed in the time series construction for the data in this study.

First an average annual cycle is computed from the monthly grid fields described in section 3 for a single overlap period between two concurrently operating satellites. We chose 1982 when there was a full-year overlap between *NOAA-6* (morning) and *NOAA-7* (afternoon). Due to its long (7+ year) lifespan, *NOAA-6* was used as a "base" to which the other satellites are ultimately calibrated.

"Anomalies" for each of the satellites were then computed from the *NOAA-6* or *NOAA-7* annual cycles (depending upon whether the satellite was either morning or afternoon), a simple subtraction of the gridpoint annual cycles from the 1982 gridpoint monthly averages. The anomalies at this point are based upon only the 1982 annual cycle of either *NOAA-6* or *NOAA-7*, without any correction for intersatellite differences.

To make the intersatellite correction, the anomalies from different satellites were compared during all periods of overlap between satellites (Fig. A1) to find the time- and gridpoint-averaged offsets relative to *NOAA-6*, which were then individually removed from each satellite's anomalies. At this point, we have anomalies that are intercalibrated between satellites but are still relative to only a single year's annual cycle (1982).

Finally, the average of 10 years of each month's anomalies was forced to zero by adding an appropriate offset to each anomaly, thus removing the 10-year mean annual cycle.

Table A1 lists 1-day and 30-day statistics of the intersatellite comparisons and adjustments, including the route of adjustment to a common level (*NOAA-6*); the dates of overlap between satellites used in the adjust-

TABLE A1. Global 1-day and 30-day statistics of all satellite overlaps between MSUs for MSU channel 2 anomalies.

Satellite	Method	Overlap dates	Number of days	Daily error (2 sat.) (°C)	Daily S/N	30-Day error (2 sat.) (°C)	30-Day S/N	Global adjustment (°C)	1-Y trend* (°C)
TIROS-N	to *NOAA-6*	7/1/79–1/19/80	149	.032	23	.012	49	+.070	+.074
NOAA-6	Base								
NOAA-7	to *NOAA-6*	6/26/81–4/16/83	552	.027	40	.004	988	+.001	+.006
NOAA-9	to *NOAA-6*	10/30/85–11/4/86	212	.025	92	.005	230	+.066	+.010
NOAA-10	to *NOAA-9*	11/26/86–3/7/87	90	.030	42	.006	372	−.284	−.063
NOAA-11	to *NOAA-10*	10/23/88–10/31/90	649	.028	39	.011	135	+.240	+.001

* Due to slightly different crossing times in afternoon satellites, there seems to be a very slight difference in annual cycles between *TIROS-N* versus *NOAA-7*. This is also seen in *NOAA-7* versus *NOAA-11*; however, the two-year overlap between *NOAA-10* and *NOAA-11* eliminates any trend due to an annual cycle in the satellite difference time series.

ments; the 1-day and 30-day standard deviation of the difference (single-satellite "error") between the overlapping satellites globally averaged channel 2 T_b anomalies; the 1-day and 30-day signal-to-noise ratios; the globally averaged net adjustment necessary to bring each satellite to the *NOAA-6* level; and the net trend in the time series of the daily differences between overlapping satellites T_b anomalies (useful for identifying potential instrumental drift in one satellite versus another). Note that the longer the period of overlap, the smaller the net trend in the difference between satellites, indicating that small random fluctuations between satellites exist on seasonal time scale but average out over a period of years. *NOAA-8* had many operational problems and was not used in any of our statistics.

REFERENCES

Conrath, B. J., 1972: Vertical resolution of temperature profiles obtained from remote radiation measurements. *J. Atmos. Sci.*, **29**, 1262–1271.

Grody, N. C., 1980: Analysis of satellite-based microwave retrievals of temperature and thermal winds: Effects of channel selection and a priori mean on retrieval accuracy. *Remote Sensing of the Atmosphere and Oceans,* A. Deepak, Ed., Academic Press, 381–410.

——, 1983: Severe storm observations with the Microwave Sounding Unit. *J. Climate Appl. Meteor.*, **22**, 609–625.

Spencer, R. W., and J. R. Christy, 1990: Precise monitoring of global temperature trends from satellites. *Science*, **247**, 1558–1562.

——, ——, and N. C. Grody, 1990: Global atmospheric temperature monitoring with satellite microwave measurements: Method and results, 1979–84. *J. Climate*, **3**, 1111–1128.